Shil'nikov homoclinic dynamics and the escape from roll autorotation in an F-4 model

M.H. Lowenberg (Department of Aerospace Engineering) &
A.R. Champneys, (Department of Engineering Mathematics)
University of Bristol, UK.

DRAFT May 29, 1998

Abstract

An investigation is undertaken into the nonlinear dynamics of an 8th-order model for the F-4J fighter aircraft in a neighbourhood of its autorotation flight regime. This regime is characterized by high roll rates with no roll control inputs. It is found that the basic state goes unstable via a supercritical Hopf bifurcation as the value of stabilator (the pitch axis control surface) is increased (i.e. control column pushed forward). The ensuing stable limit cycle behaviour is itself destroyed at a higher stabilator value in a certain homoclinic bifurcation first analysed by Shil'nikov. A careful numerical continuation analysis is performed using spline interpolation of the tabulated data in the model. The limit cycle is found to reach infinite period along a complex wiggly bifurcation curve, as predicted by the theory of Shil'nikov homoclinic orbits. Several period-doubling and secondary-Hopf (torus) bifurcations are discovered. Direct simulation of the aircraft dynamics, using linear interpolation of the data, is shown to give good agreement with the continuation results. It is found that the homoclinic bifurcation marks an escape from autorotation. That is, varying stabilator slowly through the critical value results in a jump from oscillatory autorotation to symmetric flight. Possible implications of these results for other flight phenomena are discussed.

1 Introduction

Roll-autorotation (henceforth called *autorotation* for short) is a motion of the rigid body dynamics of an aircraft that is predominantly a rapid rotation about the longitudinal axis, existing even in the absence of any roll control (aileron) input. It often takes the form of a steady motion in which the aerodynamic moments — dominated usually by regions of stalled flow which are different on the two wings — are balanced by the inertial coupling that increases in strength as rotation rates build up. In this sense it is similar to a spin but, since it develops at low angles of attack, there is usually ample control power available in order to effect a recovery.

This paper shall concern a detailed analysis of autorotation in a realistic aircraft model, upon varying a pitch axis control. The methodology used is that of bifurcation theory, for which non-specialists are referred to Glendinning (1996) or Kuznetsov (1995) for modern introductions. It will be found that the steady behaviour gives rise via a Hopf bifurcation to a mildly oscillatory form of autorotation. This periodic motion is abruptly destroyed in a global bifurcation caused by a *homoclinic orbit* of the kind first analysed by Shil'nikov (1965, 1970); see also Glendinning & Sparrow (1984), Gaspard, Kapral & Nicolis (1984), Tresser (1984), Deng (1993). Here, a homoclinic orbit, which can be thought of as an infinite-period limit cycle, is a solution that connects a *saddle-focus* equilibrium to itself. We shall seek to assess possible aeronautical implications of this method of destruction of stable autorotation behaviour. We shall also bear in mind potential application of these ideas more generally in aircraft models to recovery from other undesirable periodic motion (e.g. spin).

Earlier work by Goman & Khramtsovsky (1997) briefly discusses an autorotation mode in a simplified model — consisting of 3 ordinary differential equations (ODEs) with constant coefficients —

of a hypothetical swept-wing fighter at high altitude and supersonic speed. As in the current study, autorotation is initially steady and, as the control parameter is increased, a Hopf bifurcation appears followed by a stable limit cycle. The periodic orbit then disappears in a homoclinic connection with a saddle point. This situation is a useful 'textbook-type' example of a homoclinic bifurcation. However, in that paper, which is mainly concerned with stability region analysis, there is no investigation into the details of the bifurcation. As far as the present authors are aware, homoclinic connections in *full* aircraft models have not received any attention in the literature.

The aircraft model used in this study is a mathematical representation of the McDonnell-Douglas F-4J Phantom (Mitchell, Myers, Teper & Johnston 1980) via a system of 8 coupled ODEs with non-constant aerodynamic characteristics specified as data. This F-4 model has been used extensively by the first author in studies of non-linear aircraft behaviour (Lowenberg 1991), and more recently for novel developments associated with bifurcation tailoring (Lowenberg 1998). Although it does not represent a current state-of-the-art fighter aircraft in many respects, it has the advantage of being a relatively simple model the dynamics of which is well understood.

The rest of the paper is outlined as followed. In §2 the model equations used are given. §3 then presents the results of a numerical bifurcation analysis on a smoothed version of the model, using the continuation software AUTO (Doedel, Champneys, Fairgrieve, Kuznetsov, Sandstede & Wang (1997), Doedel, Keller & Kernevez (1991*a*, 1991*b*)). The resulting wiggly bifurcation curve of periodic orbits is shown to have excellent agreement with the predictions of Shil'nikov homoclinic bifurcation theory. §4 then presents simulation results on the model with non-smooth data, and the homoclinic orbit is found to play an organizing role in the transition from autorotation to trim symmetric flight. Finally §5 discusses the wider implications of these results.

2 The model

A standard form of the equations of motion for rigid-body aircraft in six degree of freedom flight is adopted. We follow the usual approximations for stability and control work: earth fixed in inertial space, curvature and rotation of the earth ignored, gravitational acceleration taken as constant, aircraft mass and mass distribution fixed during the time intervals of concern. Furthermore, we neglect any moving masses within the airframe (rotating engine components, dynamic effects of control surface movements). We assume that the aircraft has a plane of symmetry (left-hand side a mirror image of the right hand side, so that aerodynamic, inertial and propulsive loads are also symmetric in this sense — except, of course, when asymmetric control inputs are applied, namely non-zero rudder and/or aileron). Finally, the influence of height changes are ignored since they occur very slowly relative to the aircraft modes of motion.

Applying Newton's laws to such a system results in a set of eight ODEs, which are commonly used in open-loop rigid-body flight dynamics studies. Using a Cartesian axis system with origin at the vehicle centre of mass, the equations can be written as follows:

$$I_{xx}\dot{p} = qr(I_{yy} - I_{zz}) + I_{xz}(\dot{r} + pq) + L + L_P, \tag{1}$$

$$I_{yy}\dot{q} = rp(I_{zz} - I_{xx}) + I_{xz}(r^2 - p^2) + M + M_P, \tag{2}$$

$$I_{zz}\dot{r} = pq(I_{xx} - I_{yy}) + I_{xz}(\dot{p} + qr) + N + N_P, \tag{3}$$

$$\dot{\alpha} = q - \tan\beta(p\cos\alpha + r\sin\alpha) + \frac{Z_w + Z_P}{mV_T\cos\beta}, \tag{4}$$

$$\dot{\beta} = p\sin\alpha - r\cos\alpha + \frac{Y_w + Y_P}{mV_T}, \tag{5}$$

$$\dot{V_T} = \frac{X_w + X_P}{m}, \tag{6}$$

$$\dot{\phi} = p + q \sin\phi \tan\theta + r \cos\phi \tan\theta, \tag{7}$$

$$\dot{\theta} = q \cos\phi - r \sin\phi, \tag{8}$$

where:

g is acceleration due to gravity;
I_{xx}, I_{yy} and I_{zz} are moments of inertia about the x, y and z body axes;
I_{xz} is a cross-product of inertia;
L, M and N are the aerodynamic rolling, pitching and yawing moments (about the x, y and z axes respectively) which are in general functions of several state variables and control parameters (the latter being δ_a, δ_r and δ_{stab} in this case);
L_P, M_P and N_P are the rolling, pitching and yawing moments induced by the propulsion system (about the x, y and z axes respectively);
m is aircraft mass;
p, q and r are the roll, pitch and yaw rates (about the x, y and z axes);
V_T is total flight path velocity;
X_w, Y_w and Z_w are the axial, side and normal aerodynamic forces relative to flight path axes, which in general are functions of the state variables and control parameters;
X_P, Y_P and Z_P are the axial, side and normal propulsive forces relative to flight path axes;
α and β are the angles of attack and sideslip;
δ_a, δ_r and δ_{stab} are the aileron, rudder and stabilator control surface deflections;
ϕ and θ are the bank and pitch orientation angles respectively.

The system of equations (1)–(8) can be expressed in the generic form

$$\dot{\boldsymbol{x}}(t) = \boldsymbol{f}(\boldsymbol{x}(t), \boldsymbol{\delta}(t)), \qquad \boldsymbol{x}, \boldsymbol{f} \in \mathbb{R}^n, \qquad \boldsymbol{\delta} \in \mathbb{R}^m, \tag{9}$$

where $\boldsymbol{x}$ is a vector of n state variables (in this case $[p\ q\ r\ \alpha\ \beta\ V_T\ \phi\ \theta]^T$), $\boldsymbol{\delta}$ is a vector of m parameters $\dot{\boldsymbol{x}}$ is the time derivative of $\boldsymbol{x}$, and $\boldsymbol{f} : \mathbb{R}^n \times \mathbb{R}^m \rightarrow \mathbb{R}^n$ is the vector field (the n nonlinear functions). For this paper $\boldsymbol{\delta} = [\delta_a\ \delta_{stab}\ \delta_r]^T$ is a vector containing the three control variables, which we regard as either being steady parameters or slowly-varying presscribed functions of time.

The mass and inertial properties of the F-4 model are represented directly within equations (1) –(6), while its aerodynamic characteristics are incorporated within L, M, N, X_w, Y_w and Z_w. For the purposes of this paper, the propulsive thrust force is constant at 60 kN. Note that equations (7) and (8) are purely kinematic relationships which provide the orientation of the aircraft to the gravity vector.

The F-4J model was obtained from Mitchell et al. (1980). This is a constant Mach number version of a larger model assembled from three separate data sources to represent the full-scale aircraft's behaviour in air combat manoeuvring. The aerodynamic reactions are represented within L, M, N, X_w, Y_w and Z_w in a fairly standard manner, using the linear terms of a Taylor series expansion (with respect to the states and controls) in each case. The coefficients in these expressions (known as 'stability derivatives') are, however, not all constants: most are nonlinear functions of angle of attack α and are given in the form of data tables; there is also a term in the expression for M that is a two-dimensional table in terms of α and β. The aerodynamic model is regarded as being valid over a range of angles of attack from 0° to 110° and a sideslip range of -30° to $+30^\circ$ for the aircraft in a clean configuration (no flap, slat or undercarriage extension).

The functional dependance of the six aerodynamic reactions on state variables and control parameters for the F-4J model is as follows:

$$\begin{array}{ll} L(V_T, \alpha, \beta, p, r, \delta_a, \delta_r), & X_w(V_T, \alpha), \\ M(V_T, \alpha, \beta, q, \dot{\alpha}, \delta_a, \delta_{stab}), & Y_w(V_T, \alpha, \beta, \delta_a, \delta_r), \\ N(V_T, \alpha, \beta, p, r, \delta_a, \delta_r), & Z_w(V_T, \alpha, \delta_{stab}). \end{array}$$

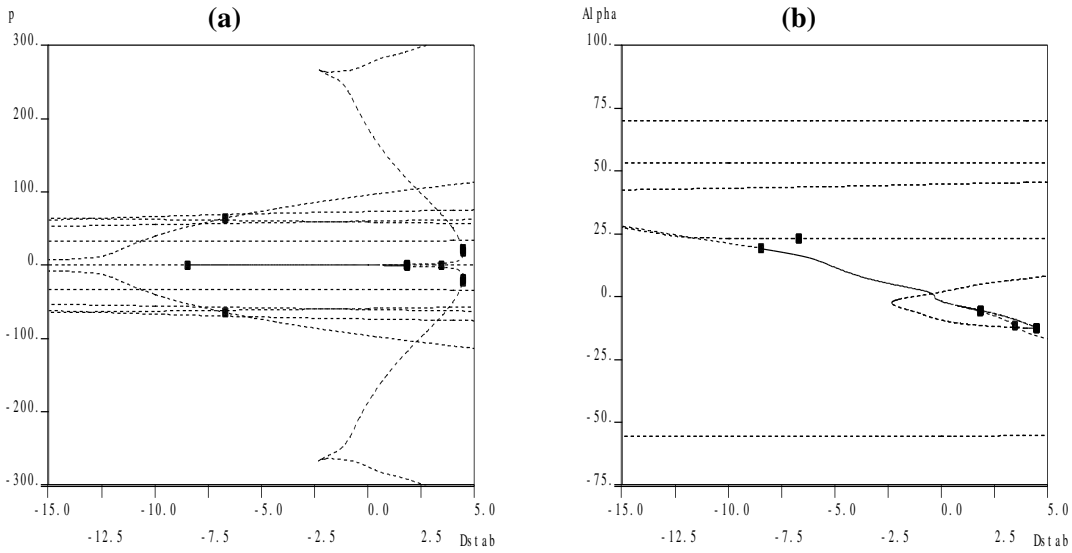

Figure 1: Overall bifurcation of equilibrium paths; **(a)** p versus δ_{stab} and **(b)** α versus δ_{stab}. Solid lines represent stable equilibria, and dashed lines unstable ones. Solid boxes represent Hopf bifurcation points. Notice from (a) that the two symmetrically-related autorotation branches are stable just to the right of the folds at $|p| \approx 265$ (note Hopf bifurcations on these braches are not depicted due to their proximity to the folds, but see Figure **??**). In (b) these two branches are overlaid and occur for low angle of attack α, so that they are hard to distinguish from the symmetric trim branch.

In this study, a slightly modified form of these tables is used: additional data points were added in order to create a smoother variation of dependent variables. This ensures that results using linear interpolation (as used in §4 below) match those generated using cubic spline fits (as in §3). The weight and inertia properties of the aircraft model correspond to a configuration with partially full internal fuel tanks, an empty centre-line tank and missile pylons on wing stations 2 and 8. A complete listing of all the data used may be found in (Lowenberg 1991). For simplicity, the analysis that follows does not include a stability augmentation system, and no input is assumed from the rudder and aileron controls ($\delta_a = \delta_r = 0$). We consider only the effect of varying stabilator δ_{stab}.

3 Numerical continuation results

In this section we have used a cubic spline interpolation of the data in (1)–(6) to define a smooth 8^{th}-order system of ODEs (9) with a single bifurcation parameter δ_{stab}. Bifurcation diagrams are computed using the software AUTO (Doedel et al. 1997); see Doedel, Keller & Kernevez (1991*a*, 1991*b*) for the methods used. Specifically we have taken the discretisation and tolerance constants `NTST` $= 100$, `NCOL` $= 4$ and `EPSL` $=$ `EPSU` $= 1.0 \times 10^{-6}$.

Figure 1 presents the overall details of the bifurcation diagram of equilibrium solutions of the model. For more details see Lowenberg (1991, 1998). Note that all angular rates (p, q, r) are in degrees/s, angles (α, β, ϕ, θ) in degrees and velocity (V_T) in m/s; period T is given in seconds.

The branch that chiefly concerns us here is the autorotation branch for roll rate $p \approx 265$. Obviously, due to symmetry, the results will equally well apply to the symmetrically opposite branch near $p = -265$. More details of this branch are presented in Figure 2(a) from which it can be seen that after a fold at $\delta_{stab} = -2.320$ there is a short region of stable equilibrium until $\delta_{stab} = -1.966$ whereupon a stable limit cycle is born in a Hopf bifurcation. The shape of a projection of this limit cycle onto the (p, α)-plane can be seen in Figure 2(b). The approximate range of oscillation of the unpresented six variables may be gleaned from Figures 6, 7 below.

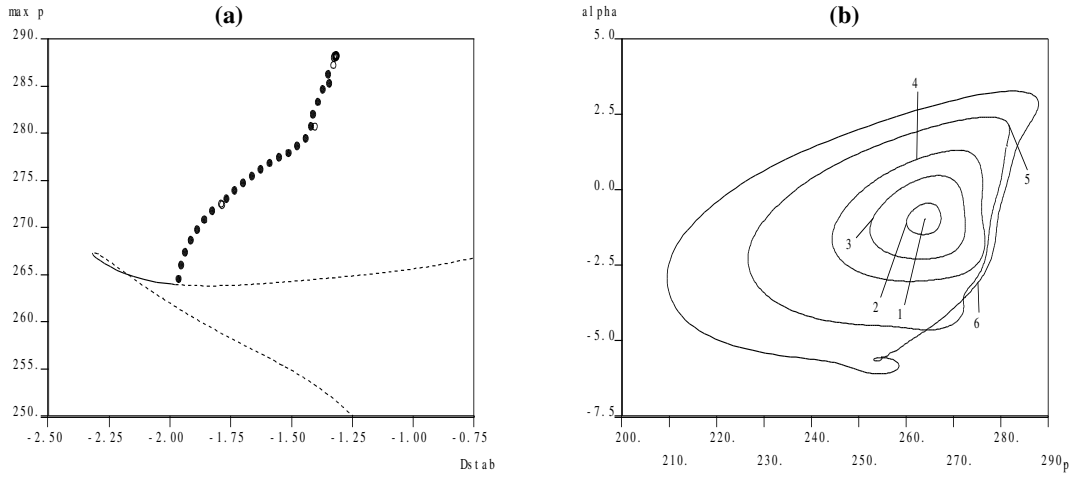

Figure 2: **(a)** Bifurcation diagram of equilibria (solid lines stable, dashed lines unstable) and limit cycles (solid circles stable, hollow circles unstable) close to the fold of the positive autorotation branch. **(b)** Projection onto the (p, α)-plane of Hopf point at $\delta_{stab} = -1.96563$ (label 1) and limit cycles at $\delta_{stab} = -1.93829$ (label 2), $\delta_{stab} = -1.79101$ (label 3), $\delta_{stab} = -1.59989$ (label 4), $\delta_{stab} = -1.41478$ (label 5), and an approximation to the homoclinic orbit at $\delta_{stab} = -1.325597$ (label 6).

As δ_{stab} is further increased to about -1.320, the limit cycle grows in amplitude to that at label 6 in Figure 2(b). Before doing so, it undergoes a sequence of bifurcations which are shown in more detail in Figure 3. Firstly, there is an apparently endless sequence of fold bifurcations of limit cycles corresponding to a Floquet multiplier passing through unity; see for example Glendinning (1996) and Kuznetsov (1995) for general information on these and other bifurcations of limit cycles. We also find other bifurcations, notably period-doublings (the creation of an orbit of double the period via a Floquet multiplier passing through -1) and Neimark-Sacker or secondary Hopf bifurcations (the creation of invariant tori composed of quasi-periodic motion via a complex pair of Floquet multipliers passing through the unit circle). Using the automatic bifurcation detection functions in AUTO, we have been able to accurately locate several of these bifurcations on the lower limbs of the curve of periodic orbits, as indicated in Figure 3(a) and (b). These result in windows of stable periodic behaviour along a branch that is otherwise unstable. However, after the first few folds AUTO is unable to detect any additional windows of stability or bifurcations other than folds. This does not exclude the possibility of self-similar bifurcation structures on these higher limbs of the wiggly curve, but with the windows of stability occuring in too small a parameter interval to be numerically detectable.

A more illuminative way of depicting what is going on along this branch of limit cycles is to plot the results as period versus parameter, as in Figure 4. Here it is clear that, although the amplitude of the limit cycle is increasing as the termination of the branch is approached, the overwhelming feature is that the period appears to be tending to infinity. This is indicative of a homoclinic orbit, where the limit cycle collides with a saddle-type equilibrium. Graphs of each component of the limit cycle for high period ($\delta_{stab} \approx -1.32$) are plotted in Figure 5. Here note that the trajectory spends a long time in a neighbourhood of

$$E : (p, q, r, \alpha, \beta, \phi, \theta, V_T) = (251.7, -63.30, -22.87, -5.801, -12.97, -109.9, -75.03, 329.4),$$

which is an equilibrium of the system at this parameter value. This equilibrium is on the lower, unstable, autorotation branch which joins the stable one at the fold (see Figure 2(a)).

Using the theory of homoclinic orbits, and the linearisation at E we are now in a position to explain the features of the wiggly curve displayed in Figure 4 and their implications for the observable dynamics. A good reference for the information we require is Glendinning & Sparrow (1984).

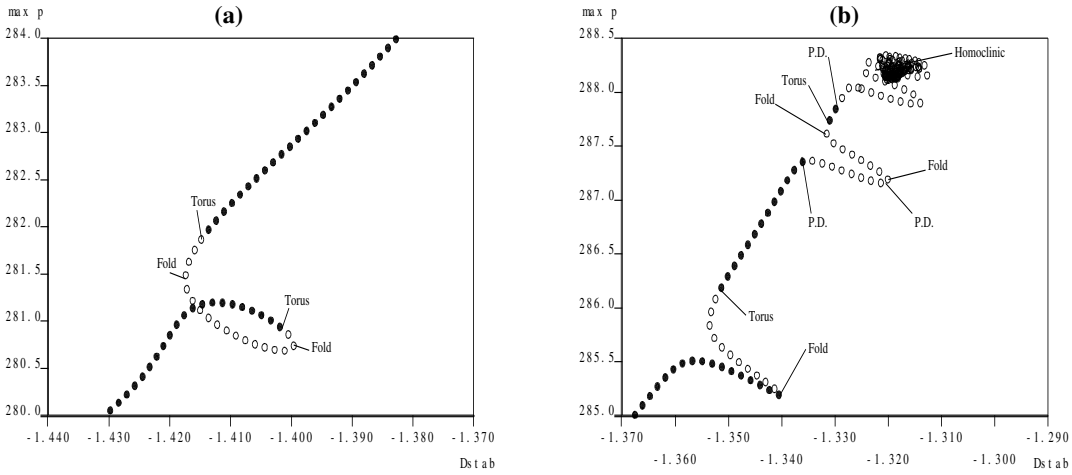

Figure 3: More details of the bifurcations occuring along the branch of limit cycles near **(a)** $\delta_{stab} \approx -1.4$ and **(b)** $\delta_{stab} \approx -1.33$. Bifurcation points computed include `Folds` of limit cycles, period-doubling (`P.D.`) bifurcations and Neimark-Sacker (secondary Hopf) bifurcations which give rise to an invariant `Torus` in the dynamics.

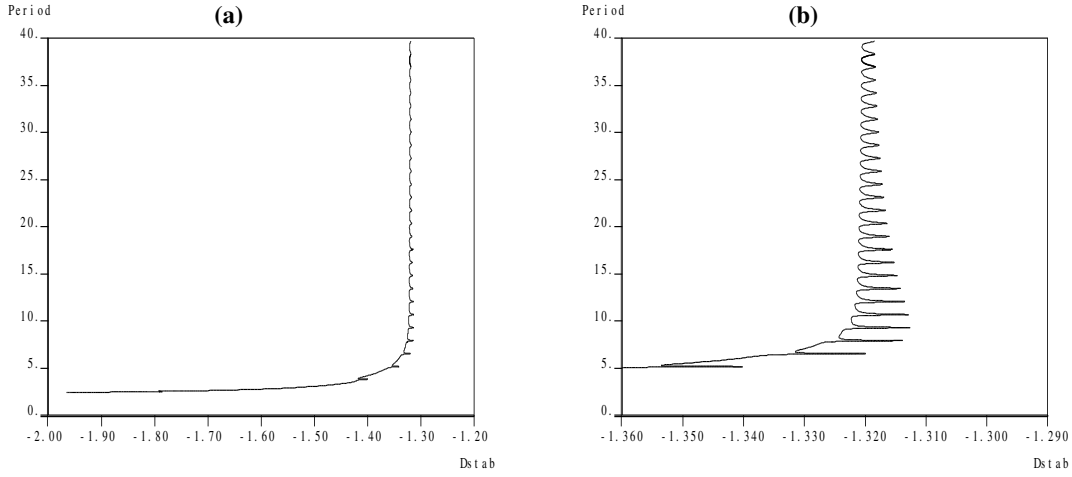

Figure 4: **(a)** The curve of limit cycles plotted as period versus δ_{stab}. **(b)** More details near the infinite-period limit $\delta_{stab} \approx -1.32$.

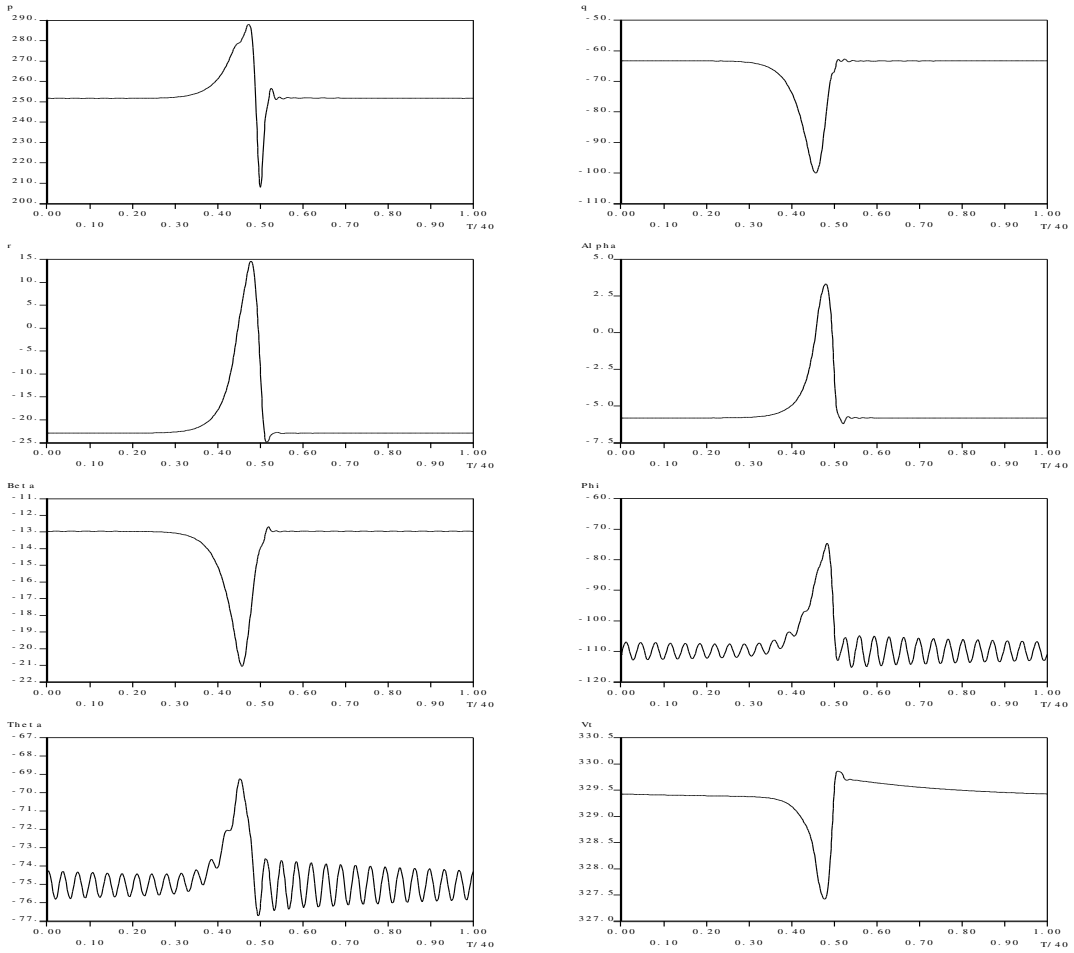

Figure 5: The eight components of a periodic orbit with period $T \approx 40$ at $\delta_{stab} = -1.31852$ which approximates the (infinite-period) Shil'nikov homoclinic orbit.

Linearising at E for $\delta_{stab} = -1.32$ we find eigenvalues

$$\begin{aligned} \lambda_1 = 0.7684, \qquad & -\lambda_2 \pm \mathrm{i}\omega_2 = -0.0291 \pm 4.548\mathrm{i}, \\ -\lambda_3 = -0.0804, \qquad & -\lambda_4 \pm \mathrm{i}\omega_4 = -1.390 \pm 8.698\mathrm{i}, \\ & \lambda_5 \pm \mathrm{i}\omega_5 = -2.912 \pm 3.833\mathrm{i}. \end{aligned}$$

These eigenvalues are found to be remarkably insensitive to the value of δ_{stab}, varying typically only in the second significant figure for δ_{stab} varying in the range $(-2, -1)$. Hence we shall refer to E as being of *saddle-focus* type because the negative-real-part eigenvalues closest to the imaginary axis are complex whereas the unstable eigenvalue is real. Moreover, the eigenvalues satisfy the inequality (in the notation of Glendinning & Sparrow (1984)) $\delta = \lambda_2/\lambda_1 < 1$. Hence Shil'nikov's theory applies, implying that in a neighbourhood of the homoclinic trajectory there are chaotic dynamics and infinitely many distinct periodic orbits (in the parlance of dynamical systems theory, this dynamics is conjugate to a shift map on infinitely many symbols). However, we cannot say that these chaotic dynamics are necessarily stable. In fact for the example here they are probably not, since the linear dynamics near E has divergence given by $\lambda_1 - 2\lambda_2$ which is positive and hence repulsive.

We can say more. Since $\delta < 1$ the calculations in Glendinning & Sparrow (1984) imply that a 'primary' periodic orbit undergoes precisely such a wiggly period versus parameter diagram as depicted in Figure 4. As the curve undergoes each successive pair of folds, so the periodic orbit gains an extra full wind in a neighbourhood of the equilibrium E. Note that such windings are most evident in the

i	**L or R**	δ_{stab}	μ_i	**period**
21	R	-1.318295	0.00188	35.5669
21	L	-1.320646	-0.00047	35.0001
15	R	-1.317527	0.00285	27.2933
15	L	-1.320838	-0.00066	26.7510

Table 1: Data at the 15th and 21st left and right fold points of the curve of periodic orbits depicted in Figure 4(a).

graphs of ϕ and θ in Figure 5 which depicts the solution after many wiggles up the curve, hence there are many oscillations of the graph around the value of E. The fact that the winds are most noticeable in these variables is presumably because the eigenvectors associated with the weakest stable eigenvectors $-\lambda_2 \pm \mathrm{i}\omega_2$ point mostly in the (ϕ, θ) direction.

The theory (Glendinning & Sparrow 1984, Sect. 3.1.2) also predicts the asymptotic shape of the wiggly curve. Let $\mu = \delta_{stab} - \delta^h_{stab}$, where δ^h_{stab} is the parameter value of the homoclinic orbit. Then let $\mu_i^{L,R}$ be the μ-value of the i^{th} fold bifurcation either to the left (L) or right (R) (counting the fold with lowest period first). Finally, let p_i be the period of the period orbit at the i^{th} intercept with $\mu = 0$. Then we have

$$\lim_{i\to\infty} (p_{i+1} - p_i) = \pi/\omega_2 = 0.6907 \tag{10}$$

$$\text{and} \quad \lim_{i\to\infty} (\mu_{i+1}^{L,R}/\mu_i^{L,R}) = \exp(-2\pi\lambda_2/\omega_2) = 0.9606. \tag{11}$$

To test these limits against the numerical data we take the two pairs of successive fold points whose data are given in Table 1. Between these pairs of folds are 10 others, 5 left-folds and 5 rights. From the way these folds accumulate as the period increases, by demanding that the rate of accumulation should be the same for left and right, we obtain that $\delta^h_{stab} = -1.320176$. This is the parameter-value we use in order to calculate μ. Using the data in Table 1, we can calculate a numerically observed value of $p_{i+1} - p_i$ twice by subtracting $p_{15}^{L,R}$ from $p_{21}^{L,R}$ and dividing by 12. Thus, we obtain 0.6894 and 0.6874 which agree well with the theoretical limit (10) as the period tends to infinity. Furthermore, we can calculate $\mu_{21}^{L,R}/\mu_{15}^{L,R}$ and take the 6^{th} root to obtain expressions for $\mu_{i+1}^{L,R}/\mu_i^{L,R}$. Here we obtain 0.9445 and 0.9445 which are close to their theoretical limit (11) as $i \to \infty$, although there is a slight discrepency.

This discrepancy may be to do with the fact that the calculations in Glendinning & Sparrow (1984) rely on the approximation by a three-dimensional vector field, spanned at E by the eigenvectors associated with λ_1 and $-\lambda_2 \pm \mathrm{i}\omega_2$. This assumption may be justified rigourously in the limit $\mu \to 0$ using the so-called 'homoclinic centre-manifold theorem' of Sandstede (1995). However, the presence of another very small stable eigenvalue $-\lambda_3$ may mean that μ has to be taken very small for the three-dimensional approximation to be valid. This may also account for the appearance of torus bifurcations along the lower limbs of the wiggly curve, which are not present in the theoretical analysis.

This careful testing of the quantitative properties of the wiggly curve in Figure 4 over a tiny range of δ_{stab}-values may seem of little significance to practical questions of aircraft dynamics. We have merely done this in order to demonstrate categorically that the observed data imply that the Shil'nikov mechanism is at work. We shall now turn to more practical questions of how this mechanism affects the aircraft's dynamics.

4 Aircraft simulation results

An existing 6 degree-of-freedom simulation of the F-4J was available for use in evaluating the implications of the autorotation dynamics. This is coded in Simulink — a program for simulation of dynamic systems that is an extension to MATLAB (Inc. 1993). Model definition is achieved via a block diagram representation, using a selection of library blocks, and MATLAB M-files. Several integration algorithms are provided, a 5^{th}-order variable-step explicit Runge-Kutta method being used in the runs generated for this paper.

The use of this simulation to investigate the time response of the aircraft model was of interest because: it was set up completely independently of the AUTO model, using the same equations and data but constructed differently; it uses linear interpolation of the data tables (splines are used in AUTO); and it provides the opportunity to observe the aircraft response to parameter sweeps—both quasi-static and more rapid to represent real flight conditions.

As a result of the different data interpolation, the values of the state variables and the parameter in the vicinity of the autorotation flight regime differ from that of spline interpolation by approximately 3–4%. The value of p in stable autorotation is about 254, as opposed to 265 for spline interpolation; and the value of δ^h_{stab} is approximately -1.28 (as against -1.320 from the AUTO results). This magnitude of discrepency was expected for solutions involving high rotation rates.

In Figure 6 the simulation is initiated in the equilibrium region of the autorotation branch, with $\delta_{stab} = -1.9$; δ_{stab} is then increased slowly to a value of -1.5 which is beyond the Hopf bifurcation and in the stable limit cycle region. The time histories confirm the presence of these two stable behaviours and hence the possibility for the aircraft to enter into this very high roll rate motion.

It is important in this study to be sure that the behaviour produced by the simulation, using linear interpolation, is in fact topologically equivalent to that generated in the numerical continuation runs. In Figure 7 the initial conditions are identical to that of Figure 6 (as is the case for all the time histories shown in this paper) but the parameter is fixed at $\delta_{stab} = -1.28145$. This parameter value is found in the simulations to be the limit of stable periodic motion near the autorotation branch for these initial conditions. Increasing δ_{stab} by 1 in the 5th decimal place results in wildly different behaviour. Note from Figure 7 that the limit cylce observed matches closely to those found in the continuation analysis approaching the homoclinic orbit (Figure 5). The limit cycle here is not quite homoclinic as it has developed only 4 or so oscillations close to E rather than infinitely many (but do note the transient in Figure 7 appears much closer to being homoclinic). The precise mechanism for loss of stability of limit cylces in the simulations may well be one of the bifurcations (fold, period-doubling or torus) that the continuation analysis found to occur close to the homoclinic orbit (see Figure 3). Nevertheless it would be fair to say that the simulations indicate that the homoclinic orbit plays a strong role in the destruction of the autorotation stable limit cycle behaviour.

In the event of an aircraft entering roll autorotation, the pilot will need to know what control actions bring about a recovery to stable trimmed flight conditions. Decreasing δ_{stab} will ensure that the fold bifurcation is encountered, such that the autorotation branch ceases to exist and recovery to the stable symmetric branch is effected (see Figure 1). Now that the presence of the homoclinic bifurcation is known, it is expected that recovery from autorotation can also be induced by *increasing* the parameter. Such a case is shown in Figure 8, where δ_{stab} is increased in steps from -1.9 to zero. Again, both the stationary point and the limit cycle portions of autorotation are evident; but once δ_{stab} exceeds a certain value (which is approximately -1.28144 under quasi-static conditions but is lower when the parameter increases at a finite rate) the limit cycle quickly disappears and there is a jump to the symmetric trim branch (running the simulation for longer, ϕ and θ do eventually damp out to their expected steady states).

The behaviour exhibited in the time history in Figure 8 conforms to the predictions that could be made from Figure 1, namely the likelihood of the jump to stable equilibirium. Figure 1 also shows that for $\delta_{stab} > 2$ the symmetric trim branch is no longer stable. Any attempt by a pilot to escape from

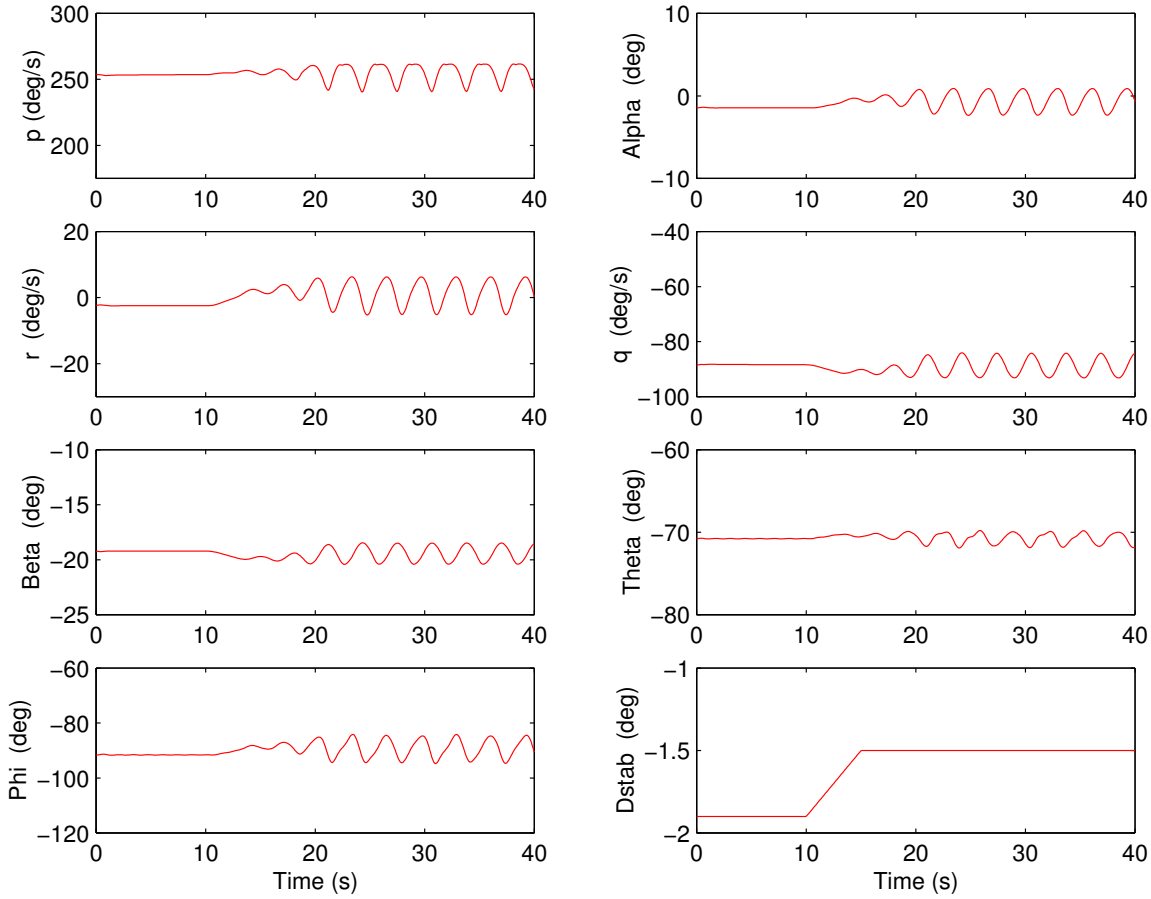

Figure 6: The first seven components of the motion (the forwards velocity V_T is approximately constant throughout this and all subsequent runs) given the depicted variation of δ_{stab}. The initial value of δ_{stab} is -1.9, where the autorotation equilibrium is stable, and the final value is $\delta_{stab} = -1.5$ where the limit cycle is stable. Initial conditions for this and all subsequent runs are $p = 254.0$, $q = -88.5$, $r = -2.47$, $\alpha = -1.44$, $\beta = -19.22$, $\phi = -91.6$, $\theta = -70.78$, $V_T = 314.0$.

autorotation by increasing δ_{stab} can be expected to result in an undesirable outcome should the increase in parameter be too large. This is verified in the time histories in Figure 9, which are identical to those in Figure 8 except that δ_{stab} is stopped at $+2.5$ instead of 0. The result is a series of oscillations of extemely high amplitude in all variables, which will impose severe loads on the aircraft and pilot. The nature of this behaviour appears to be chaotic—probably arising from the interaction of two (or more) of the unstable equilibria evident in Figure 1 at $\delta_{stab} = 2.5$. Recovery from this highly undesirable state to stable symmetric conditions has been shown (using simulation) to be possible by moving δ_{stab} to a value less than 2.

5 Discussion

The above results demonstrate the existence of stable autorotation in the F-4J model and characterise its dynamic properties in terms of regions of equilibria and of stable periodic orbits. They also reveal the exact nature of the homoclinic bifurcation through which the limit cycle collides with a saddle equilibrium point and disappears. The conditions under which autorotation is possible are therefore clear, as are the means of recovery via variation of the parameter δ_{stab}.

This type of analysis is clearly of benefit in understanding the flight dynamics characteristics of an aircraft. The fidelity with which the aerodynamic model represents the actual aircraft is always

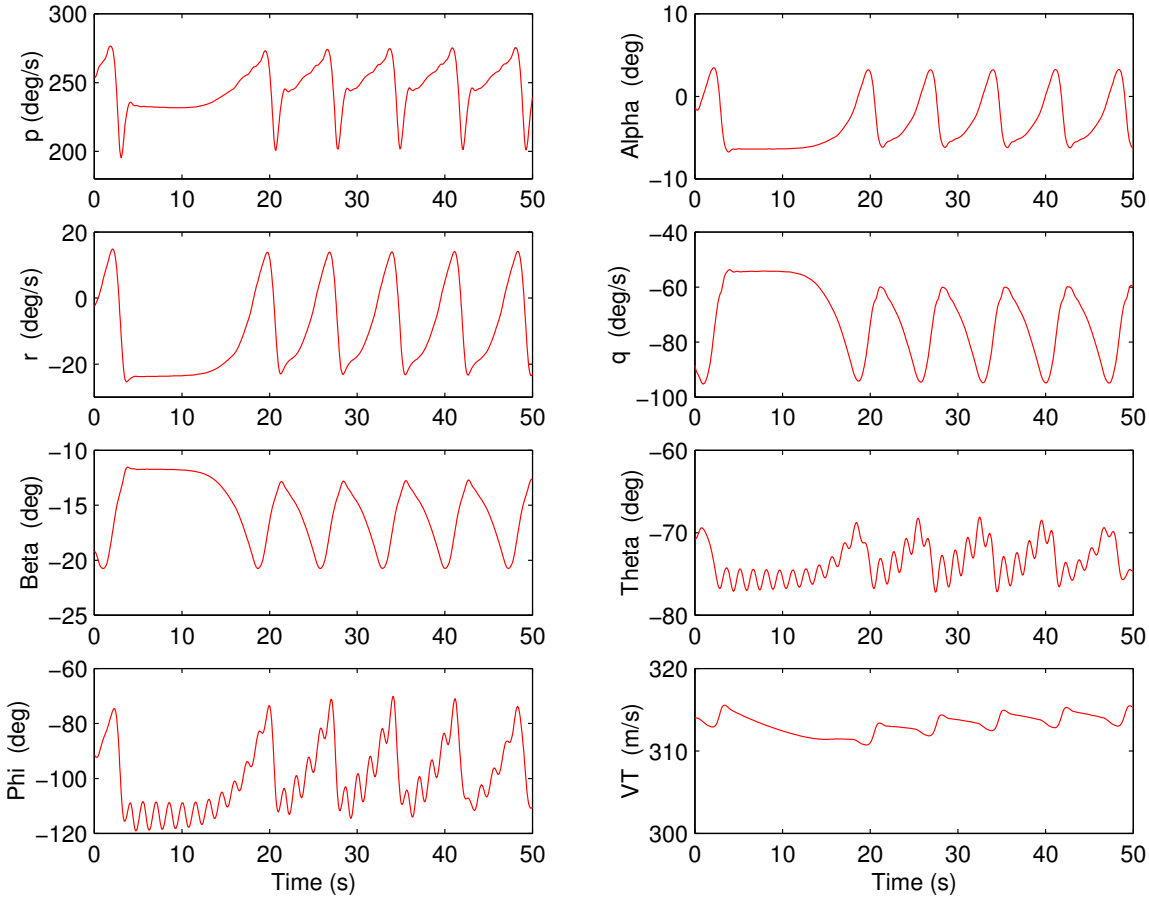

Figure 7: The eight components of motion at fixed $\delta_{stab} = -1.28145$.

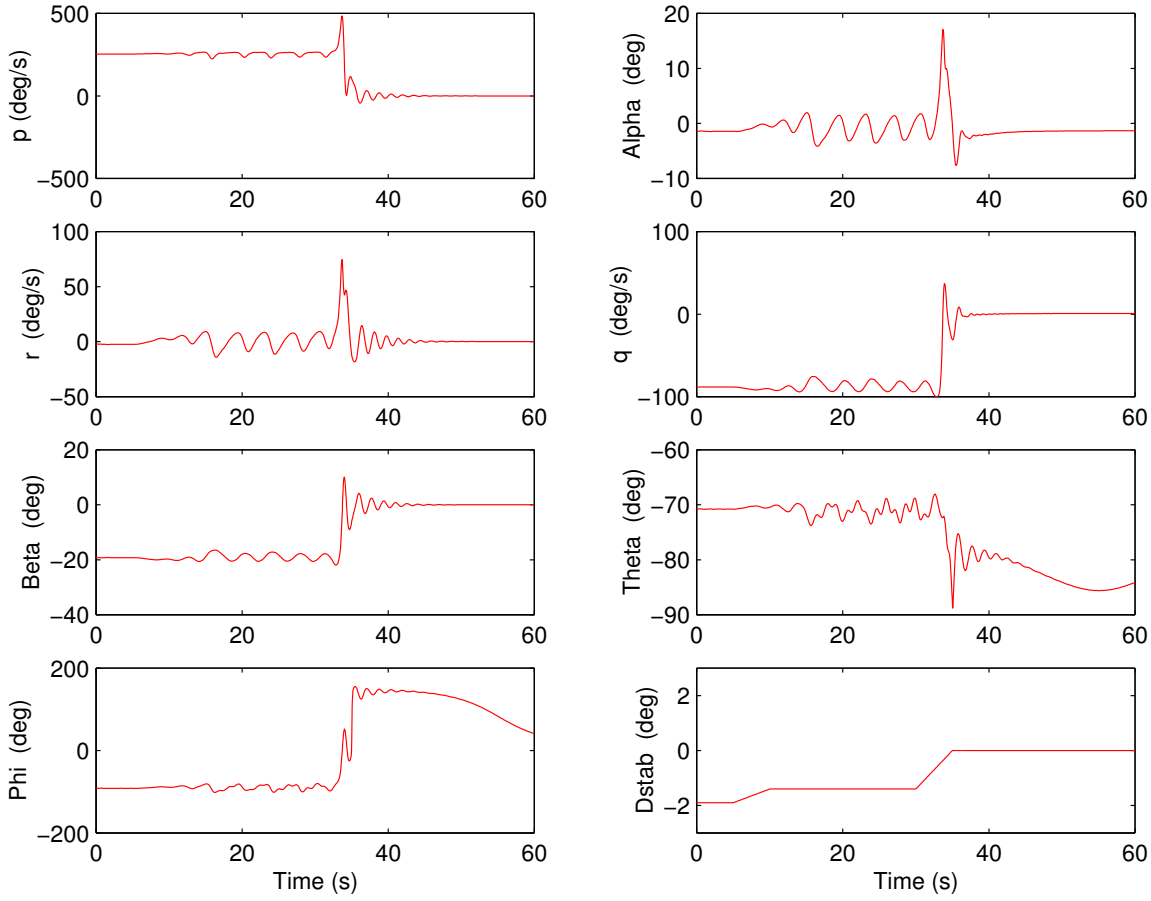

Figure 8: The first seven components of the motion given the depicted variation of δ_{stab}. The three constant values are $\delta_{stab} = -1.9$ at which the autorotation equilibrium is stable, $\delta_{stab} = -1.4$ where there is a complex limit cycle, and $\delta = 0$ which is after the autorotation limit cycle has disappeared via the homoclinic orbit, but before the symmetric trim branch has lost stability.

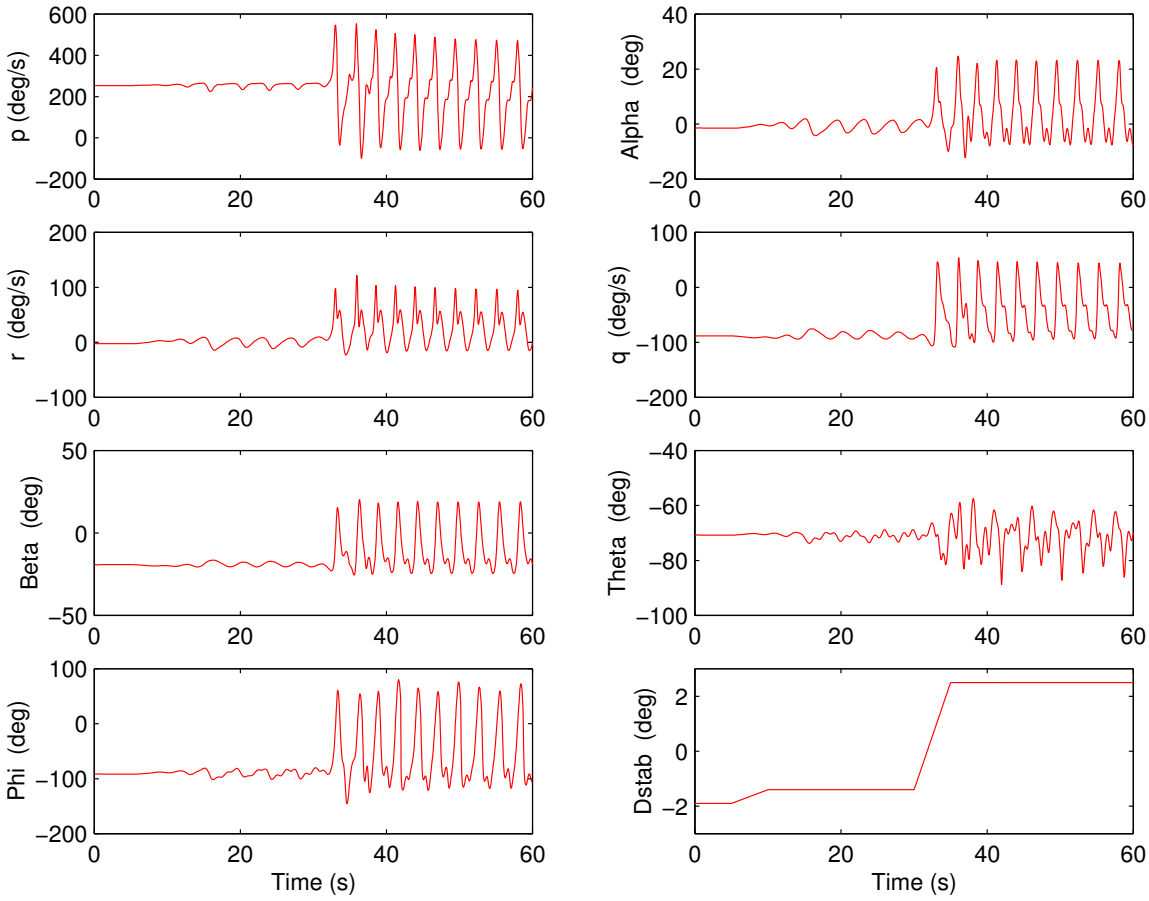

Figure 9: Similar to Figure 8 but the final value of $\delta_{stab} = 2.5$ is such that the symmetric trim branch is no longer stable.

of concern in such studies: there are likely to be significant unsteady effects during these high-rate motions, particularly in the oscillatory regions, which may not be faithfully captured in the F-4J mathematical model. Nevertheless, it is known that many aircraft do possess an autorotation mode and, since it is sustained by a balance between aerodynamic and inertial loads, the results obtained for the F-4J model are likely to be a reasonable reflection of its roll rotation dynamics.

The importance of the current study is that, whatever level of accuracy of aerodynamic reactions is incorporated within the ODEs, numerical continuation can be used to provide an in-depth understanding of the system dynamics. The application of the technique in the context of homoclinic connections need not necessarily be restricted to autorotation. Many aircraft possess oscillatory spin modes which are periodic orbits and it is conceivable that spin recovery could be effected by creating the conditions for the limit cycle to collide with an unstable equilibrium branch—possibly via the sort of 'bifurcation tailoring' proposed in Lowenberg (1998). It is also possible that the wing rock limit cycle, which is common to most fighter aircraft, may in some situations end up in a homoclinic connection; the disappearance of the limit cycle could then correspond to *lateral-directional departure*, which usually occurs if wing rock is permitted to continue to higher α. In this case, it would be useful to tailor the phase portrait so as to move a saddle or saddle-focus equilibrium *further away* from the limit cycle thus delaying the homoclinic bifurcation. If this were achievable, then wing rock could be extended over a wider operating region which might be advantageous since it is usually easier to control than departure.

In the case of the F-4J, the autorotation conditions may well persist under variation of δ_a—a longitudinal-axis control device used to induce roll motions. This possibility deserves further investigation, since the phenomena observed in this paper would then be of interest not purely in a restricted autorotative flight regime but over a range of conditions in which high-roll-rate motion is demanded. There, knowledge and possible tailoring of the behaviour of limit cylces around the equilibrium branch may enable even higher roll-rate manoevers to be attempted.

References

Deng, B. (1993), 'On Shil'nikov's saddle-focus theorem', *J. Diff. Eqs.* **102**, 305–329.

Doedel, E., Champneys, A., Fairgrieve, T., Kuznetsov, Y., Sandstede, B. & Wang, X. (1997), 'AUTO97 continuation and bifurcation software for ordinary differential equations'.

Doedel, E., Keller, H. & Kernevez, J. (1991*a*), 'Numerical analysis and control of bifurcation problems: (I) bifurcation in finite dimensions', *Int. J. Bifurcation and Chaos* **1**, 493–520.

Doedel, E., Keller, H. & Kernevez, J. (1991*b*), 'Numerical analysis and control of bifurcation problems: (II) bifurcation in infinite dimensions', *Int. J. Bifurcation and Chaos* **1**, 745–772.

Gaspard, P., Kapral, R. & Nicolis, G. (1984), 'Bifurcation phenomena near homoclinic orbits: a two-parameter analysis', *J. Stat. Phys.* **35**, 697–727.

Glendinning, P. (1996), *Stability, instability and chaos: an introduction to the theory of nonlinear differential equations*, Cambridge University Press, Cambridge.

Glendinning, P. & Sparrow, C. (1984), 'Local and global behaviour near homoclinic orbits', *J. Stat. Phys.* **35**, 645–696.

Goman, M. & Khramtsovsky, A. (1997), Global stability analysis of nonlinear aircraft dynamics, *in* 'AIAA Atmospheric Flight Mechanics Conference Technical Papers', AIAA-97-3721-CP, American Institute of Aeronautics and Astronautics, USA, pp. 662–672.

Inc., T. M. (1993), *Simulink Dynamic System Simulation Software User's Guide*, USA.

Kuznetsov, Y. A. (1995), *Elements of Applied Bifurcation Theory*, Springer-Verlag, New York, U.S.A.

Lowenberg, M. (1991), *Application of the Bifurcation Analysis Technique to Aircraft Dynamics*, Master's thesis, University of the Witwatersrand, South Africa.

Lowenberg, M. (1998), 'Bifurcation analysis of multiple-attractor flight dynamics', *Phil. Trans. R. Soc. Lon. A.*

Mitchell, D., Myers, T., Teper, G. & Johnston, D. (1980), *Investigation of High Angle of Attack Maneuver-Limiting Factors – Part III: Appendix I*, Technical report, Systems Technology Inc., Technical Rept. AFWAL-TR-80-3141 Part III, USA.

Sandstede, B. (1995), Center manifolds for homoclinic solutions, Technical report, Weierstraß Institut für Angewandte Analysis und Stochastik. Preprint No. 186, submitted to *J. Dyn. Diff. Eqns.* .

Shil'nikov, L. (1965), 'A case of the existence of a countable number of periodic motions', *Sov. Math. Dokl.* **6**, 163–166.

Shil'nikov, L. (1970), 'A contribution to the problem of the structure of an extended neighborhood of a rough equilibrium state of saddle-focus type', *Mat.* USSR *Sb.* **10**, 91–102.

Tresser, C. (1984), 'About some theorems by L.P.Sil'nikov', *Ann. Inst. Henri Poincare* **40**, 441–461.